




Article

Simulation of Reinforced Reactive Injection Molding with the Finite Volume Method

Florian Wittemann ^{1,*}, Robert Maertens ², Alexander Bernath ¹ , Martin Hohberg ¹, Luise Kärger ¹ and Frank Henning ^{1,2}

¹ Karlsruhe Institute of Technology (KIT), 76131 Karlsruhe, Germany; alexander.bernath@kit.edu (A.B.); martin.hohberg@kit.edu (M.H.); luise.kaerger@kit.edu (L.K.); frank.henning@ict.fraunhofer.de (F.H.)

² Fraunhofer Institute of Chemical Technology (ICT), 76327 Pfinztal, Germany; robert.maertens@ict.fraunhofer.de

* Correspondence: florian.wittemann@kit.edu; Tel.: +49-721-60845379

Received: 19 December 2017; Accepted: 22 January 2018; Published: 31 January 2018

Abstract: The reactive process of reinforced thermoset injection molding significantly influences the mechanical properties of the final composite structure. Therefore, reliable process simulation is crucial to predict the process behavior and relevant process effects. Virtual process design is thus highly important for the composite manufacturing industry for creating high quality parts. Although thermoset injection molding shows a more complex flow behavior, state of the art molding simulation software typically focusses on thermoplastic injection molding. To overcome this gap in virtual process prediction, the present work proposes a finite volume (FV) based simulation method, which models the multiphase flow with phase-dependent boundary conditions. Compared to state-of-the-art Finite-Element-based approaches, Finite-Volume-Method (FVM) provides more adequate multiphase flow modeling by calculating the flow at the cell surfaces with an Eulerian approach. The new method also enables the description of a flow region with partial wall contact. Furthermore, fiber orientation, curing and viscosity models are used to simulate the reinforced reactive injection molding process. The open source Computational-Fluid-Dynamics (CFD) toolbox OpenFOAM is used for implementation. The solver is validated with experimental pressure data recorded during mold filling. Additionally, the simulation results are compared to commercial Finite-Element-Method software. The simulation results of the new FV-based CFD method fit well with the experimental data, showing that FVM has a high potential for modeling reinforced reactive injection molding.

Keywords: reinforced reactive injection molding; thermoset processing; process simulation; FVM; OpenFOAM

1. Introduction

Reinforced reactive injection molding (RRIM) is one of the most important manufacturing processes for short fiber reinforced composites with thermoset matrices. The process significantly affects the mechanical and optical properties of the final part. Hence, the process control is crucial for manufacturing high performance parts. Furthermore, an adequate process simulation is needed to achieve this process control and fulfill the high standards of the automotive and polymer industry [1–5].

Despite the importance of the RRIM process, well-known simulation software is often focused on thermoplastic injection molding and uses the same models for RRIM. However, thermosets show a more complex flow behavior, triggered by a low-viscosity surface layer resulting from the hotter mold [1,2,5]. Furthermore, the flow is not shear dominated, like a plug flow, which is a typical adoption for thermoplastics [1,2]. Additionally, commercial software does not simulate the air in the mold as a separate flow phase. This simplification is made to reduce the calculation time, but consequently

neglects phenomena like air traps with significant influence on the process. These are only taken into account with empirical models in the post processing. For good simulation of RRIM, many material and process aspects need to be considered. As the resin is a non-Newtonian fluid, the viscosity must be modeled as function of temperature, shear rate and degree of cure to accurately simulate the pressure field [6]. For that purpose, and to have a reliable prediction of cycle time, curing kinetics have to be modeled in addition to rate-dependent viscosity models. Furthermore, fiber orientations should be predicted, since they have a significant influence on the mechanical and thermal properties of the final part [3,4,7].

On the one hand, commercial software is often based on the Finite-Element-Method (FEM) to simulate the RRIM process [8–11]. On the other hand, Finite-Volume-based solvers, representing the state of research, focus on thermoplastic injection molding using incompressible and isothermal models [12]. In this study, the Finite-Volume-Method (FVM) is used, resolving the flux at the cell faces and using an Eulerian approach [13–15]. Due to this flow modeling, FVM provides a more realistic multiphase flow with physical significance on the fluxes, which is not possible in FEM by solving a Lagrangian mesh at the nodes. For implementation and simulation, the open source Computational-Fluid-Dynamics (CFD) toolbox OpenFOAM 4.1 (OpenCFD Ltd., Bracknell, UK) [7,12–15] is used and well-known viscosity, curing and fiber orientation models are implemented to model the reinforced reactive injection molding process. A solver for compressible, non-isothermal multiphase flow is extended, using a phase depending boundary condition, defined to enable mold-filling simulation, by separating and interpolating boundary conditions for polymer and air. Additionally, the solver predicts fiber orientation, resulting from the flow during mold filling.

The simulation results are compared to a commercial FEM software (Moldflow 2018.1, Autodesk, San Rafael, CA, USA) and to experimental injection molding trials of a glass fiber reinforced phenolic resin.

2. Models and Implementations

The following subsections present the models and methods used for phase-dependent boundary conditions, curing kinetics, viscosity and fiber orientation. The models are implemented in OpenFOAM 4.1, using C++ as the program language and finite volume theory for the numerical solution [13–15]. In principal, the Navier-Stokes equations can be solved on structured and unstructured meshes. Due to the open source code of the CFD toolbox OpenFOAM, several solvers for scalar transport, transient problems, multiphase problems etc. are available and can be extended in a user-defined way.

In the present work, a new solver is created for mold filling simulation of fiber reinforced thermoset materials. The new solver is based on the compressible, non-isothermal multiphase solver compressibleInterFoam. This solver uses the Volume-of-Fluid-Method (VoF) for modeling multiphase flows. VoF separates the different phases using the dimensionless scalar α , which is equal to one in cells completely filled by phase 1, zero in cells filled with phase 2 and $0 < \alpha < 1$ in the interface regions [13,15]. In this work, $\alpha = 1$ means that a control volume is completely filled with polymer resin, and $\alpha = 0$ if it is filled with air. The boundary conditions of the injection flow are accordingly extended to phase-dependent formulations. Additionally, material models for curing kinetics, viscosity and fiber orientation are implemented to suitably model the reinforced reactive flow behavior.

2.1. Governing Equations

The governing equations are the continuity equation, momentum and energy balance to form the Navier-Stokes equations.

The continuity equation describes the change of the density ρ as follows:

$$\frac{d\rho}{dt} + \frac{\partial(\rho U_i)}{\partial x_i} = 0, \quad (1)$$

where incompressibility is not assumed, so $\frac{d\rho}{dt} = 0$ is not generally applicable and U_i is the velocity vector.

For momentum balance the general formulation

$$\frac{d\rho U_i}{dt} + \frac{\partial(\rho U_i U_j)}{\partial x_j} = -\frac{\partial p}{\partial x_i} + \eta \frac{\partial U_i}{\partial x_j \partial x_j} \quad (2)$$

is used with p being the pressure and η being the viscosity (see Section 2.4).

The energy balance describes the distribution of the temperature T with:

$$\frac{d\rho T}{dt} + \frac{\partial(\rho U_i T)}{\partial x_i} = \frac{\lambda}{c_p} \frac{\partial T}{\partial x_i \partial x_i}, \quad (3)$$

according to Fourier's law. The parameters λ and c_p are thermal conductivity and specific heat capacity in this case. The wall temperature of the mold is assumed to be constant, hence no heat transfer between the material and the mold is needed. Radiation is neglected.

2.2. Phase-Dependent Boundary Condition

Three types of boundary faces can be distinguished in OpenFOAM: An inlet for flow into the system, an outlet for flow out of the system and a wall, which cannot be passed by any media. To enable mold-filling simulation, a special boundary condition (BC) for the outlet is developed, which allows the air phase, but not the polymer phase, to leave the mold through the outlet face. Hence, the outlet BC for velocity vector \mathbf{U} is implemented as an interpolation between a Dirichlet boundary condition, defining the absolute value of \mathbf{U} to be zero, and a Neumann boundary condition, defining the gradient of \mathbf{U} to be zero. The interpolation depends on the VoF factor α , in such a way that a cell completely filled with polymer has a pure Dirichlet BC and a cell completely filled with air has a pure Neumann BC. Consequently, the boundary face changes from an outlet to a wall during filling, represented by:

$$BC = \alpha \cdot \text{DirichletBC} + (1 - \alpha) \cdot \text{NeumannBC}, \quad (4)$$

with

$$\text{DirichletBC} \stackrel{\text{def}}{=} \mathbf{U} = \begin{pmatrix} 0 \\ 0 \\ 0 \end{pmatrix} \text{ and } \text{NeumannBC} \stackrel{\text{def}}{=} \frac{d\mathbf{U}}{dt} = \begin{pmatrix} 0 \\ 0 \\ 0 \end{pmatrix}. \quad (5)$$

For implementation of the phase-dependent BC, a GroovyBC is used, which is part of the third party tool SWAK4FOAM 0.4.1 (Free Software Foundation, Boston, MA, USA). The program code is described in Appendix A.

2.3. Model for Curing Kinetics

Modeling of curing kinetics is an important aspect since cross-linking significantly influences the viscosity and consequently the process pressure and cycle time [16,17]. In this study, the Kamal-Malkin model is used to model curing kinetics, since it is a well-known and often used model for curing kinetics of thermoset polymers [11,16–21]. The model describes the cure rate by

$$\frac{dc}{dt} = (K_1 + K_2 c^m)(1 - c)^n \quad (6)$$

with

$$K_1 = A_1 \exp\left(-\frac{E_1}{R \cdot T}\right), \quad (7)$$

$$K_2 = A_2 \exp\left(-\frac{E_2}{R \cdot T}\right), \quad (8)$$

where c is the degree of cure between 0 and 1, R is the ideal gas constant and m, n, A_1, E_1, A_2, E_2 are material specific constants which have to be identified by experimental measurements like Differential Scanning Calorimetry (DSC) and curve fitting [17]. The curing heat is neglected because of the thin part geometry, hence the curing kinetics have no influence on the temperature distribution. The reaction kinetics model is implemented as a thermo-chemical model within the OpenFOAM structure.

2.4. Model for Viscosity

The Castro-Macosko viscosity model [6] is an often used and well-established model to simulate the viscosity of thermoset materials [11,20,21]. The model describes the viscosity as a function of temperature T , shear rate $\dot{\gamma}$ and degree of cure c :

$$\eta(T, \dot{\gamma}, c) = \frac{\eta_0(T)}{1 + \left(\frac{\eta_0(T)\dot{\gamma}}{\tau^*}\right)^{(1-n)}} \left(\frac{c_g}{c_g - c}\right)^{(c_1+c_2 \cdot c)} \quad (9)$$

and

$$\eta_0(T) = B \cdot \exp\left(\frac{T_b}{T}\right), \quad (10)$$

with τ^*, n, c_1, c_2, B and T_b being material specific constants. c_g denotes the material specific degree of cure at gelation. The Castro-Macosko model is implemented as a transport model in the thermo-physical model library of OpenFOAM.

2.5. Model for Fiber Orientation

For calculation of the fiber orientations, the Folgar Tucker model is used [22–25]. A well-described implementation of this model has already been published by Kerstin Heinen [7]. Heinen’s code is extended in the present work to model multiphase flows. Hence, fiber orientation is calculated only in cells with $\alpha \geq 0.5$. In all other cells the initial conditions remain. The result is a symmetric tensor [23], with the diagonal entries being the probability of fibers oriented in this coordinate direction with a value between zero and one, where zero means no fibers are aligned in this direction and one, that all fibers are aligned in this direction. The summation of the diagonal entries must be equal to one.

The fourth order fiber orientation tensor $A_{kl ij}$ is described by second order tensors using the hybrid closure approximation, as described in [7,23,24]. The differential equation for the second order fiber orientation tensor in a control volume is given by:

$$\frac{dA_{ij}}{dt} + \frac{\partial v_i A_{jk}}{\partial x_k} = -\left(W_{ik} A_{kj} - A_{ik} W_{kj}\right) + \lambda_F \left(D_{ik} A_{kj} - A_{ik} D_{kj} - 2D_{kl} A_{kl ij}\right) + 2C_I \dot{\gamma} (\delta_{ij} - 3A_{ij}), \quad (11)$$

with

$$D_{ij} = \frac{1}{2} \frac{\partial U_i}{\partial x_j} + \frac{1}{2} \left(\frac{\partial U_i}{\partial x_j}\right)^T \quad (12)$$

$$W_{ij} = \frac{1}{2} \frac{\partial U_i}{\partial x_j} - \frac{1}{2} \left(\frac{\partial U_i}{\partial x_j}\right)^T \quad (13)$$

$$\lambda_F = \frac{r^2 - 1}{r^2 + 1} \quad (14)$$

where C_I is the interaction coefficient calculated with the Bay’s equation [7] and r is the aspect ratio of the fibers defined as quotient of fiber length and diameter. The vector v is the flux of the velocity vector.

3. Test Setup for Experimental Validation

3.1. Test Structure and Process Conditions

The thermoset molding compound used for the experimental studies is a phenolic resin of the novolac type, reinforced with glass fibers. The material was provided for the trials by SBHPP Vyncolit (Gent, Belgium).

For the experimental study, an electrically heated plate mold equipped with pressure and temperature sensors is used. It is a symmetrical two-cavity mold with a variable plate thickness between two and five millimeters. For the experimental studies described here, a constant wall thickness of 2 mm is chosen. Both plates have a square shape with an edge length of 190 mm. The sprue has a start diameter of 9 mm (inlet), expands to 15.5 mm and is 185 mm high. Figure 1 shows the complete molded part with sprue system. The position of the pressure and temperature sensors in one of the mold cavities is shown in Figure 2.

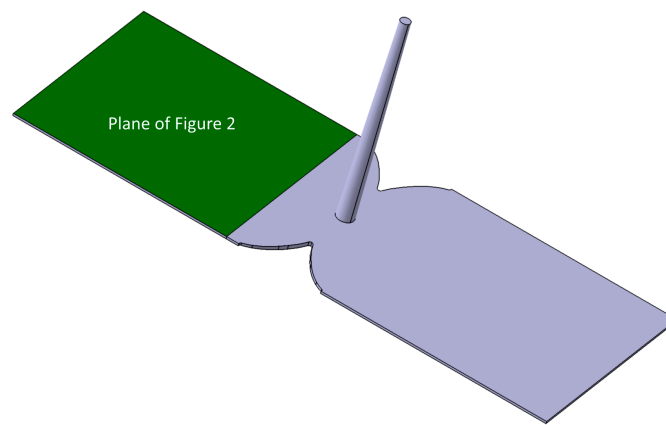


Figure 1. Molded part with sprue system.

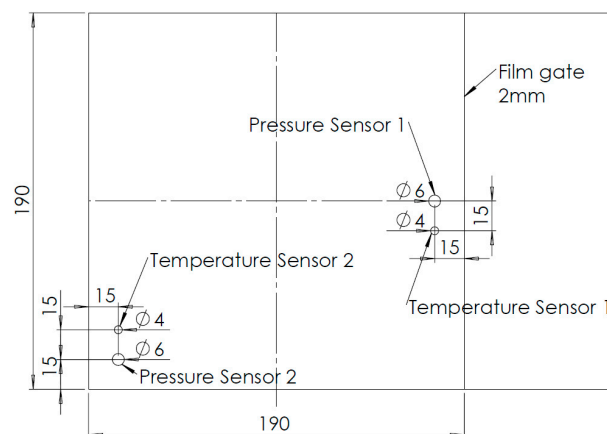


Figure 2. Position of pressure and temperature sensors in mold.

The sensor positions are in the region where the first material should appear after entering the plate mold (position 1) and the last region where material should appear before complete filling (position 2). The positions are chosen to see when the plate filling starts and ends. The sensors are nearly in plane with the mold, so the influence on material flow behavior can be neglected. For pressure measurement, sensors of the type 6163 manufactured by Kistler Instrumente GmbH (Winterhur, Switzerland) are used. These sensors are equipped with a diaphragm in order to resist the low viscosity resin. The temperature sensors are Kistler type 6192 NiCr-Ni thermocouples.

The injection molding machine is a KraussMaffei 550/2000 GX (Munich, Germany) equipped with a standard 60 mm thermoset screw without a non-return valve. The temperature control of the plasticizing unit is realized using four individually controlled, oil-tempered zones. The clamping unit has a maximum clamping force of 5500 kN.

The process parameters for obtaining the pressure and temperature signals are summarized in Tables 1 and 2.

Table 1. Constant process parameters used in the RRIM study.

Parameter	Value	Unit
Plasticizing unit temperature profile from inlet to nozzle	60–70, 70–80, 80–90	°C
Screw speed	40	1/min
Back pressure	40	bar
Switchover point	5	cm ³
Hold pressure stage 1	800	bar
Time period of stage 1	30	s
Hold pressure stage 2	800–15 (linear)	bar
Time period of stage 2	10	s
Curing time period	40	s

Table 2. Varied parameters used in the RRIM study.

Parameter	Value Min	Value Max	Unit
Mold temperature	170	190	°C
Injection speed	137.5	250	cm ³ /s
Dosage volume	230	232	cm ³

The filling is injection speed controlled until the switchover point, meaning that there is a constant material inflow until 5 cm³ of the dosage volume remains in the plasticizing unit. After the switchover, a constant pressure (hold pressure) acts on the inlet. After the hold pressure stages, the mold is separated from the plasticizing unit and no material flow in the mold is possible. The curing time ensures the shape stability of the composite part.

The aim of this study is to investigate the flow behavior with dependence on varying mold temperature and injection speed and, thus, to validate the proposed FVM-based CFD method. In order to compensate the difference in material backflow at higher injection speeds, the dosage volume is adapted accordingly. The purpose of this adaptation is to keep the maximum cavity pressure constant within the study.

3.2. Numerical Model, Boundary Conditions and Model Parameters

Since the mold is symmetric in two directions (cf. Figure 1), only a quarter of the mold is simulated to reduce the computation time. The model with predefined boundary face types is shown in Figure 3. To replicate the experiments, four simulations with different process settings are conducted. Thus, two different injection speeds and two different mold temperatures are modeled. For pressure validation, the FVM-based solver is compared to the experimental results and also to FEM results. The FEM simulations are conducted with Autodesk Moldflow Insight 2018.1, also using Castro-Macosko viscosity and the Kamal-Malkin kinetic model [8–10]. The FEM model is meshed in Moldflow with a global edge length of 3.06 mm and eight elements over thickness. The FVM model is meshed with the OpenFOAM meshing tools BlockMesh and snappyHexMesh. Therefore, a base mesh with an edge length 2 mm is used, the refinement of all surfaces is set to level 2 and one additional surface layer is created.

The initial values of the internal field and the different boundary types of faces are given in Tables 3–6.

The hydrostatic pressure is given by the scalar p_{rgh} . In this study it is equal to the pressure p , because gravity is neglected.

At the symmetry planes the symmetry condition is set for every field variable. The flow rate at the inlet in Table 4 equals one quarter of $137.5 \text{ cm}^3/\text{s}$ and $250 \text{ cm}^3/\text{s}$, because only one quarter of the mold is simulated. According to the experiments, the filling simulation is initially volume-flux controlled (Table 4), and pressure-controlled after the first switchover point. Two switchover points are also used in the FEM and FVM simulations, where the FVM settings are chosen according to the FEM simulations: After the first switchover point, the pressure is set constant at the actual values, calculated for this time step. After the second one, the pressure is set according to the holding pressure of the experiments, see Table 1. At the first switchover point, the inlet boundary condition for the velocity is changed to `pressureInletOutletVelocity`, so that the velocity is calculated relating to the fixed pressure. The switchover points are calculated from the experimental parameters and the mold volume. They are given in Table 7.

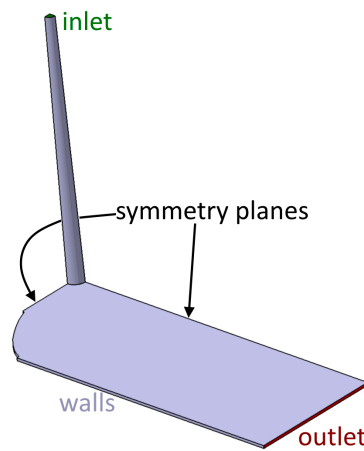


Figure 3. Finite-Volume-Method (FVM) model for OpenFOAM with boundary faces.

Table 3. Initial conditions and values for the internal field.

Field Variable	Value	Unit
A (fiber tensor)	$\begin{pmatrix} 0.33 & 0 & 0 \\ 0 & 0.33 & 0 \\ 0 & 0 & 0.33 \end{pmatrix}$	-
α	0	-
c	0.001	-
cure rate	0	1/s
$\dot{\gamma}$	0	1/s
p and p_{rgh}	10^5	Pa
T	443.15 or 463.15	K
U	(0 0 0)	m/s

Table 4. Boundary conditions and values for the inlet.

Field Variable	Type	Value	Unit
A (fiber tensor)	fixedValue	$\begin{pmatrix} 0.33 & 0 & 0 \\ 0 & 0.33 & 0 \\ 0 & 0 & 0.33 \end{pmatrix}$	-
α	fixedValue	1	-
c	zeroGradient	-	-

Table 4. Cont.

Field Variable	Type	Value	Unit
cure rate	zeroGradient	-	1/s
$\dot{\gamma}$	zeroGradient	-	1/s
p and p_{rgh}	fixedfluxPressure	10^5	Pa
T	fixedValue	423.15	K
U	flowRateInletVelocity	34.375×10^{-6} or 62.5×10^{-6}	m^3/s

Table 5. Boundary conditions and values for the outlet.

Field Variable	Type	Value	Unit
A (fiber tensor)	zeroGradient	-	-
α	zeroGradient	-	-
cure	zeroGradient	-	-
cure rate	zeroGradient	-	1/s
gammadot	zeroGradient	-	1/s
p and p_{rgh}	zeroGradient	-	Pa
T	fixedValue	443.15 or 463.15	K
U	BC (see Section 2.2)	-	m/s

Table 6. Boundary conditions and values for the wall.

Field Variable	Type	Value	Unit
A (fiber tensor)	zeroGradient	-	-
α	zeroGradient	-	-
cure	zeroGradient	-	-
cureRate	zeroGradient	-	1/s
gammadot	zeroGradient	-	1/s
p and p_{rgh}	fixedfluxPressure	10^5	Pa
T	fixedValue	443.15 or 463.15	K
U	noSlip	-	m/s

For fiber orientation prediction, a fiber volume fraction of 0.35 and an aspect ratio of 25 are assumed.

Table 7. Switchover points of the simulations.

Filling Rate	First Point	Second Point
137.5 cm ³ /s	1.46 s	1.5 s
250 cm ³ /s	0.8 s	0.82 s

Table 8 summarizes the parameter values of reaction kinetics of the material system used for experimental validation.

Table 8. Parameters for the Kamal-Malkin kinetic model.

Parameter	Value	Unit
R	8.3144598	J/(K·mol)
A1	1.9454×10^{12}	1/s
A2	3041.4	1/s
E1	2,878,805.64	J/mol
E2	38,425.6452	J/mol
m	1.643	-
n	0.4893	-

The parameter values of the viscosity model of the material system used for experimental validation are given in Table 9. Air is assumed to be a perfect gas.

Table 9. Parameters for the Castro-Macosko viscosity model.

Parameter	Value	Unit
τ^*	0.79	Pa
n	0.5	-
c_1	17	-
c_2	17	-
B	1.123×10^{-7}	Pa·s
T_b	13.750	K
c_g	0.4	-

Values received from manufacturer.

3.3. Numerical Model for Verification of Fiber Orientations

For comparison of fiber orientation results of FVM and FEM a different geometry is regarded. To verify all room directions, a mold with dominant flow in every direction is created. The boundary types are the same as mentioned in Tables 5–8. Geometry and boundary faces are shown in Figure 4.

For the velocity, an injection speed of $3.8 \text{ cm}^3/\text{s}$ is chosen, leading to a filling time of 1 s. The inlet and outlet are squares with an edge length of 5 mm. The FEM mesh is built up in Moldflow with tetrahedral elements, while hexahedral volumes created with BlockMesh are used for the FVM mesh. In both meshes a global edge length of 1 mm is set.

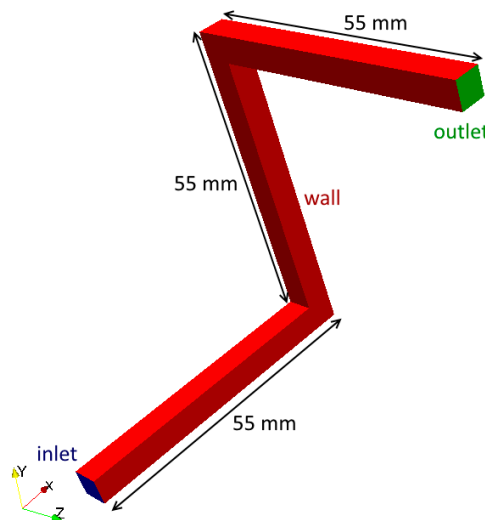


Figure 4. Geometry for fiber orientation validation.

4. Results

In this section, the simulation results are presented and compared to experimental and FEM results.

4.1. Results of the Filling Simulation

Figure 5 shows the FVM simulation results for a filling rate of $137.5 \text{ cm}^3/\text{s}$ and a mold temperature of $170 \text{ }^\circ\text{C}$. Displayed are (from top to bottom) the filling level (via VoF), the velocity in m/s and the pressure in MPa at 1 s (Figure 5a), where the filling is velocity-controlled, and at 1.5 s (Figure 5b), where it is pressure-controlled and should be just filled.

At 1.5 s the mold is not filled completely, visible at the corners, where air is still left in the system (blue). For a sum of α over all cells, divided by the total number of cells, the value should be equal to one for a complete filled system. In this case, the value is 0.998, which matches a filling state of 99.8%. The 0.2% air can be neglected and the mold is regarded as completely filled. The mold gets completely filled during holding pressure stage 1. There is no possibility to make a statement when exactly the mold in the trials is filled completely, because the material can only be detected at the sensor points. Based on the pressure data, the pressure rise and difference between sensor 1 and 2 in the trials, the filling also takes approximately 1.5 s for an injection speed of $137.5 \text{ cm}^3/\text{s}$ in the experimental studies (see Section 4.2).

A detailed look at the flow front (Figure 5a top) displays that there is no sharp interface between polymer and air, but an interface region with $0 < \alpha \leq 1$ over a few cells. This area indicates the region with partial wall contact, which is a typical phenomenon of RRIM, although a clear line between partial and full wall contact is not detectable as described in [1,2,5]. This phenomenon cannot be observed in the FEM simulation, where a sharp interface is predicted and an element is always either polymer or empty, see Figure 6.

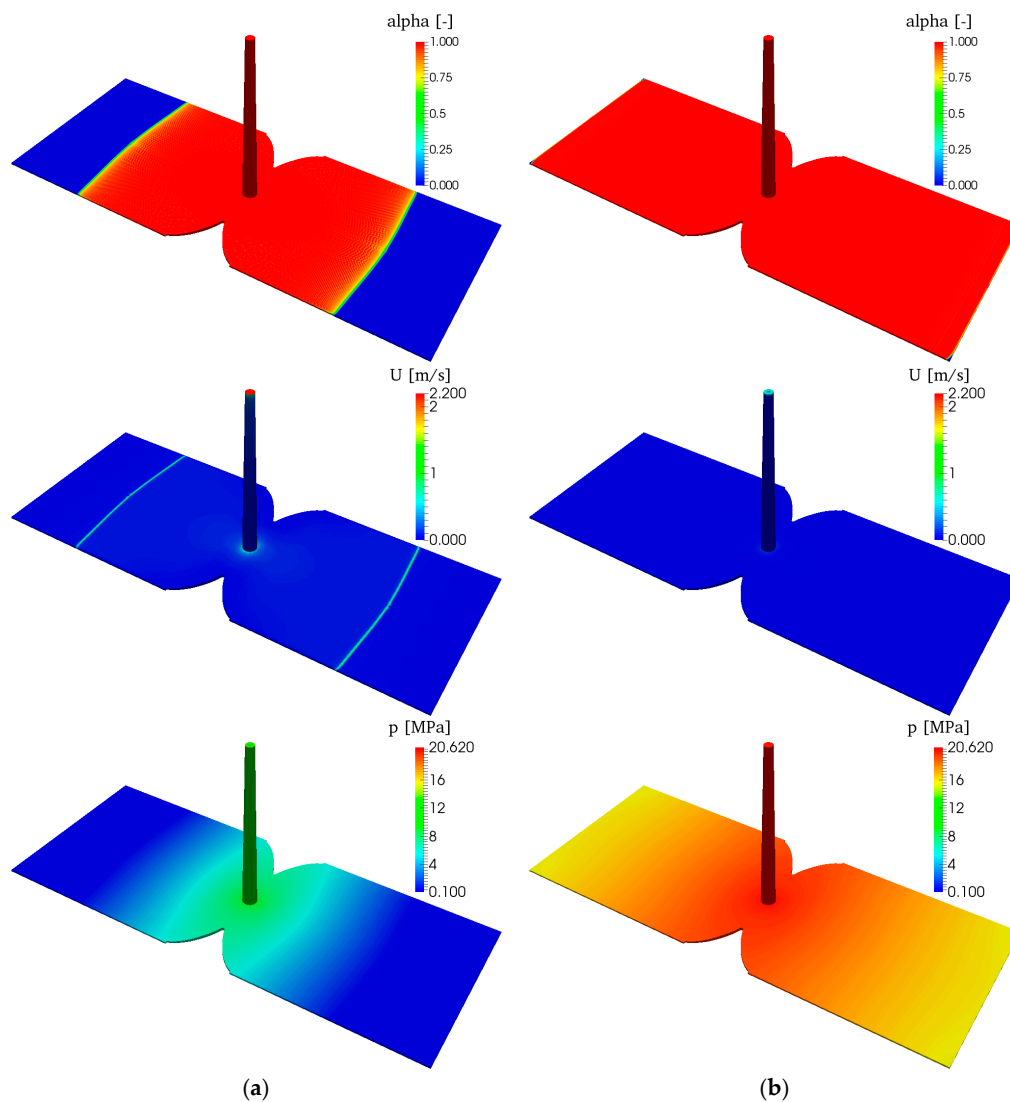


Figure 5. FVM-simulation results of polymer filling state α (top), velocity U in m/s (middle) and pressure p in MPa (bottom) after 1 s (a) and 1.5 s (b) for a filling rate of $137.5 \text{ cm}^3/\text{s}$ and a mold temperature of $170 \text{ }^\circ\text{C}$.

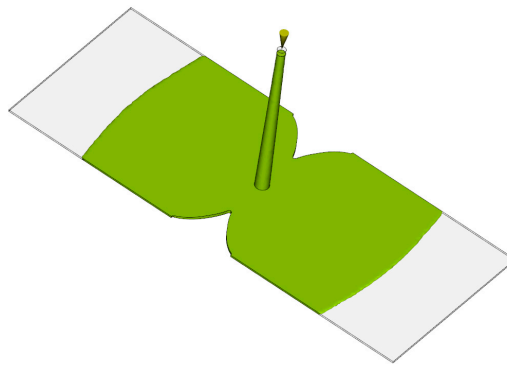


Figure 6. Filling state of the FEM-simulation at 1 s.

The velocity (Figure 5 middle) ranges in a reasonable spectrum. The polymer enters the mold with an injection speed of 2.2 m/s at the inlet, which corresponds to a volumetric flow rate of 137.5 cm³/s based on the inlet area. Furthermore, it can be seen that the velocity is nearly zero after 1.5 s (Figure 5b middle), although there is still a pressure gradient at that moment (Figure 5 bottom). This aspect approves the phase-dependent boundary condition, which stops the flow when the mold is filled.

4.2. Comparisson of Pressure

The pressure during filling with an injection speed of 137.5 cm³/s is shown in Figure 7a for a mold temperature of 170 °C and Figure 7b for 190 °C. The experiments at 170 °C are more reproducible than the ones at 190 °C, as visualized by the scatter beams in Figure 7. The large scatter at 190 °C might be caused by the fact that 190 °C is the maximum temperature for injection molding according to the manufacturer. Every curve of sensor position 1 shows a continuous pressure growth during filling (0–1.46 s). After filling, the experimental curves of sensor 1 and 2 are nearly identical, which shows good process control and filling behavior. The simulation results of FEM and FVM considerably differ from each other. Compared to measurements at sensor 1, FEM predicts a higher pressure, while the FVM results fit better to the experiments and are just slightly higher for 170 °C. At sensor 2, a significant pressure rise after switchover (1.46 s) is detectable in experiments as well as in FEM and FVM simulations. However, both simulations show a too fast pressure rise at sensor 2 compared to the measurements.

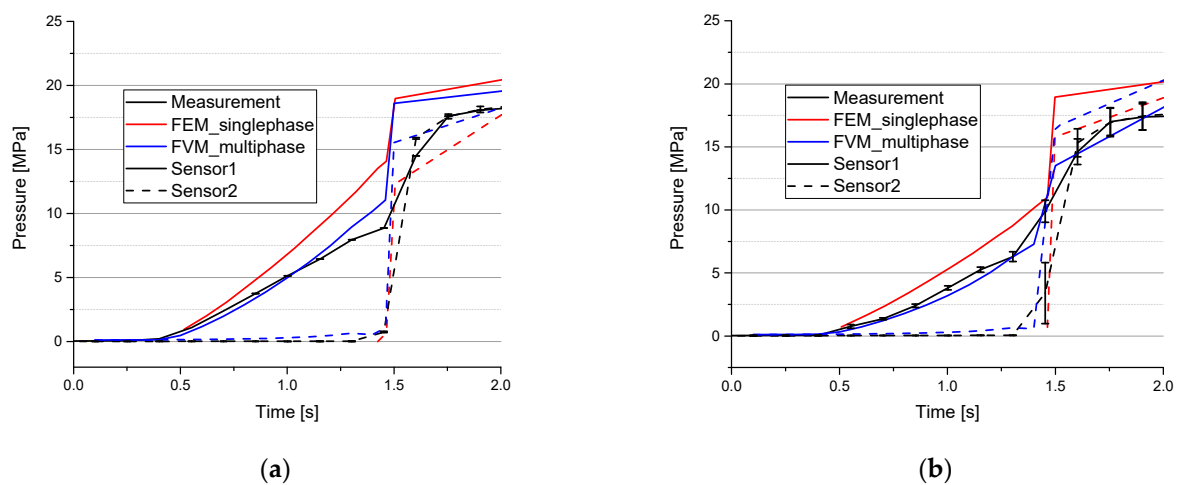


Figure 7. Pressure over time for a filling speed of 137.5 cm³/s and a mold temperature of 170 °C (a) and 190 °C (b). Comparing measurement (black), FEM (red) and FVM (blue) at sensor position 1 (solid line) and 2 (dotted line).

The pressure difference between sensor 1 and 2 after switchover is too high in both simulations for both temperatures, where it is even higher in the FEM than in the FVM calculations. In general, the pressure during filling is lower at 190 °C than for 170 °C in experiments and simulations. This is caused by the lower viscosity, resulting from the higher temperature.

Although material backflow is not simulated, the overall pressure rise at both sensor positions is quite similar in experiments and simulations. Hence, material backflow could be neglected, although no non-return valve is used in the experimental trials.

For a filling rate of 250 cm³/s, there is also a greater scatter in pressure measurement for 190 °C (Figure 8b) than for 170 °C (Figure 8a) and the pressure is again lower at 190 °C because of the lower viscosity. Up to the first switchover, the experimental data of a filling rate of 250 cm³/s show a higher pressure growth during filling than the data of the filling rate of 137.5 cm³/s (Figure 7), which is a consequence of the higher velocity. Hence, there is no visible pressure rise at switchover (0.8 s) for sensor 1. After switchover, the experimental curves of sensor 1 and 2 do not immediately fit to each other as well as for 137.5 cm³/s. For 190 °C the measured pressure at sensor 2 is even higher than the one at sensor 1 between 0.85 and 1 s.

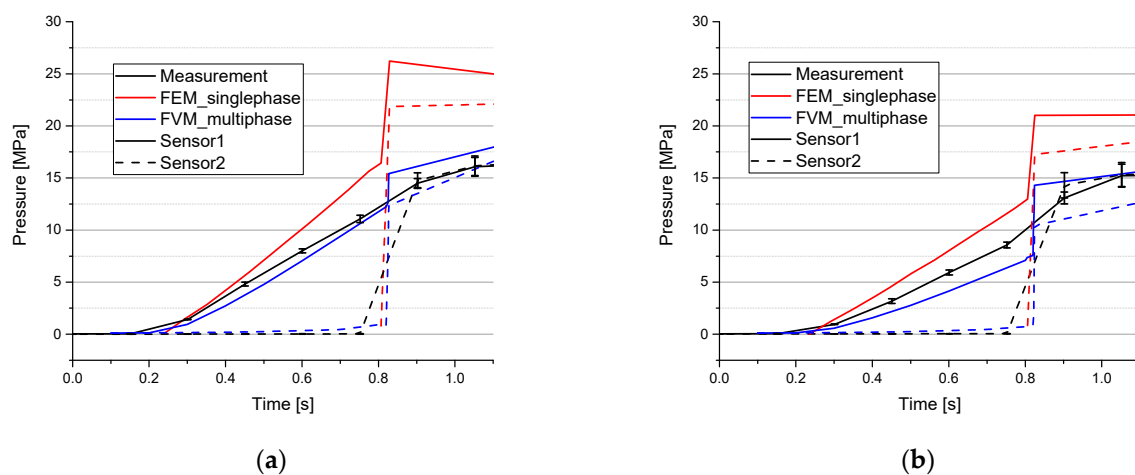


Figure 8. Pressure as a function of time for a filling speed of 250 cm³/s and a mold temperature of 170 °C (a) and 190 °C (b). Comparing measurement (black), FEM (red) and FVM (blue) at sensor Position 1 (solid line) and 2 (dotted line).

Both simulation methods overestimate the pressure rise at switchover, which is distinctly higher in the FEM simulations. As before, the FEM calculated pressure is too high for sensor 1. The pressure distribution of the FVM simulation fits well during filling for 170 °C and is too low for 190 °C. Regarding the curve course of sensor 2, the pressure rise of both methods appears too fast. However, the real pressure curve in this area is not entirely known, because there are only measure points at 0.75 and 0.9 s (switchover at 0.8 s), making the distribution look flatter.

In summary, the results of the FVM simulation are satisfying, although no further material characterization has been done except for the material data provided by the manufacturer. By ranging in a correct spectrum and rising at the right time, the FVM simulation results show a good agreement with the experimental data. The proper pressure modeling indicates a suitable viscosity modeling and hence a suitable simulation of curing kinetics, as further evaluated in the following section.

4.3. Comparison of Curing Kinetics

The correct implementation of the curing kinetics modeling of the new FVM-solver is verified by comparison with commercial FEM software, which also uses the Kamal-Malkin model. The increase of the curing degree at sensor position 1 is illustrated in Figure 9. The results are quite similar for FEM and FVM, confirming the correct implementation in the curing kinetics modeling in the FVM-solver.

At the end of filling (1.5 s) the degree of cure is about 0.85% (in the FVM simulation). This raises the viscosity by 44.5% (Equation (9)) related to the same temperature and shear rate but with a degree of curing equal to zero ($c = 0$).

The kinetic model (see Section 2.3) only depends on the state variables time and temperature, which are not as much influenced by flow as pressure and velocity. That might be the reason for the good fitting results of FEM and FVM.

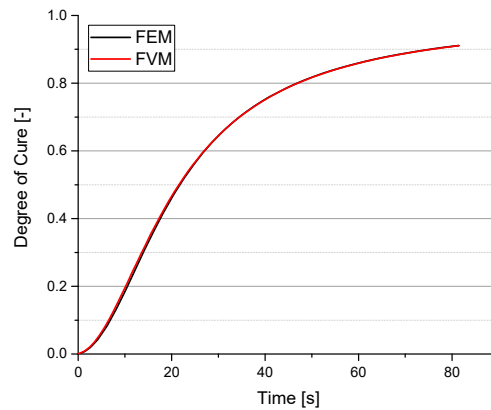


Figure 9. Degree of cure as a function of time for FEM (black) and FVM (red) for a filling speed of $137.5 \text{ cm}^3/\text{s}$ and a mold temperature of $170 \text{ }^\circ\text{C}$.

4.4. Comparison of Fiber Orientation

The fiber orientation computed by FVM simulation is compared to those of commercial FEM software. For the FEM simulation, the Moldflow standard model (Moldflow-rotation-diffusion) is chosen. The results are based on the geometry of Figure 4. The geometries in Figure 10 might seem to be different for FEM and FVM, which is only caused by the perspective.

Regarding the fiber alignment in x -direction (Figure 10a), a deviation especially in the edges can be detected. In the FEM model, a high orientation right at the beginning can be detected, while the FVM result aligns only after a few millimeters. The results in y -direction fit well, while in z -direction the FVM-solver predicts a slightly higher alignment of about 10%. The FVM solution has a higher scattering in the transition area.

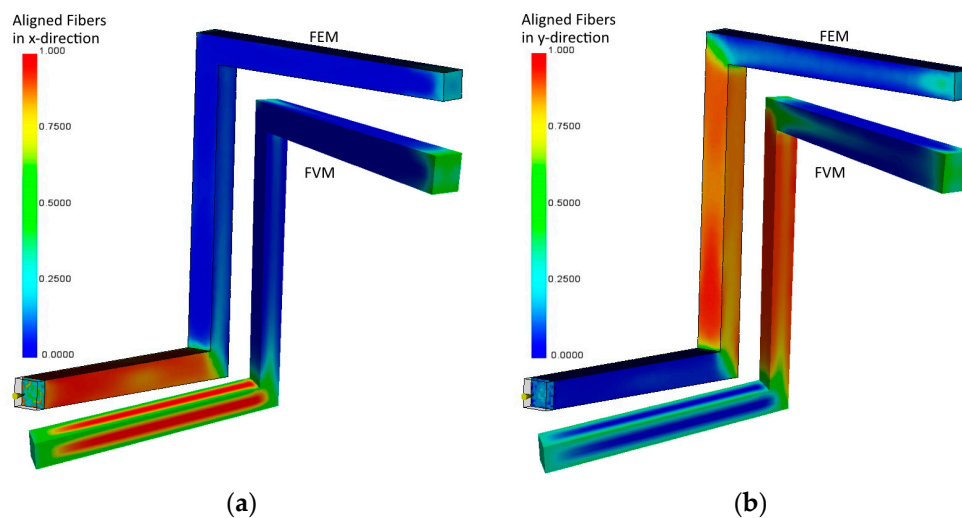


Figure 10. Cont.

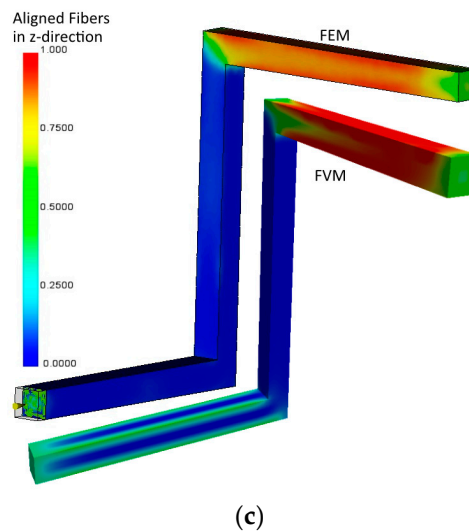


Figure 10. Comparison of predicted fiber orientation between FEM and FVM in x -direction (a), y -direction (b) and z -direction (c).

These slight differences may be caused by the different flow modeling. The plug flow, modeled in FEM, allows a faster orientation especially in regions near the walls (like edges and corners) because of the full wall contact, whereas the fountain flow with partial wall contact modeled in FVM does not lead to such a rapid orientation, because of the different velocity gradient. In summary the results fit well, which confirms a correct implementation.

5. Discussion and Conclusions

A new method for simulation of reinforced reactive injection molding is presented. The solver is implemented in the open source CFD toolbox OpenFOAM, using the Finite-Volume-Theory. Compressible, non-isothermal multiphase flows are simulated, modeling air and polymer in the mold at every iteration. Comparison with experimental data proves that the FVM-solver is able to predict pressure distribution during mold filling for several filling speeds and mold temperatures. This validates a good viscosity and flow modeling. Regions with partial wall contact are detectable at the flow front, which is a typical phenomenon of RRIM and cannot be seen in the FEM simulations. Furthermore, the new FVM-based solver simulates fiber orientation and curing kinetics at the level of commercial FEM software. Hence, this study shows the encouraging opportunity of FVM for simulation of reaction injection molding with a realistic two-phase flow modeling for thermoset materials.

The open source structure of OpenFOAM in combination with the good quality of the results achieved so far, reveal a high potential for additional features, applications and process phenomena, which can be regarded and simulated in the future. For example, diffusion and transport models can be used for analyzing the arising weld lines. The energy balance can be extended with a source term for curing heat, to have a better temperature and hence better curing and viscosity modeling for thick parts. Moreover, anisotropic viscosity models and viscoelastic behavior for modeling extensional flows can be implemented. This could lead to a better simulation of the region with partial wall contact, which is fundamental for accurate and detailed flow modeling of RRIM, having an impact on the filling, fiber orientation and hence the mechanical and thermal properties of the final part.

Acknowledgments: We would like to thank the Vector Foundation, Stuttgart, Germany for the financial support and SBHPP Vyncolit, Gent, Belgium for providing the material and the material data.

Author Contributions: Florian Wittemann performed the major part of the work in terms of method development and implementation. He also wrote the first draft of the paper. The curing kinetic and viscosity model was implemented by Alexander Bernath. All experimental work was conducted by Robert Maertens. Martin Hohberg

initiated the work, supported the FE-based simulations and revised the paper. Luise Kärger supervised the method development in general, supported the discussion of simulation results and thoroughly revised the paper. Frank Henning supervised the work in terms of composite process knowledge and relevance of the addressed subjects.

Conflicts of Interest: The authors declare no conflict of interest.

Appendix A

For implementation of the phase-dependent boundary condition, the third party tool SWAK4FOAM must be installed. The following code for the boundary condition must be placed in the **U** file of the 0 folder (or other corresponding time folders) in the boundary field block. In this case it is specified for a patch called “outlet”.

```
outlet
{
    type          groovyBC;
    aliases       {alpha1 alpha.polymer;}
    valueExpression "vector(0,0,0)";
    gradientExpression "vector(0,0,0)";
    fractionExpression "alpha1";
    value uniform (0 0 0);
}
```

Furthermore, the relevant library must be read at the end of the ControlDict file:

```
libs ("libgroovyBC.so");
```

References

1. Michaeli, W.; Hunold, D.; Kloubert, T. Formfüllung beim Spritzgießen von Duroplasten. *Plastverarbeiter* **1992**, *43*, 42–46.
2. Thienel, P.; Hoster, B. Ermittlung der Füllbildkonstruktion. *Plastverarbeiter* **1992**, *43*, 36–41.
3. Höer, M. *Einfluss der Material- und Verarbeitungseigenschaften von Phenolharzformmassen auf die Qualität Spritzgegossener Bauteile*; Universität Chemnitz: Chemnitz, Germany, 2014.
4. Englich, S. *Strukturbildung bei der Verarbeitung*; Universität Chemnitz: Chemnitz, Germany, 2015.
5. Ohta, T.; Yokoi, H. Visual analysis of cavity filling and packing process in injection molding of thermoset phenolic resin by the gate-magnetization method. *Polym. Eng. Sci.* **2001**, *41*, 806–819. [[CrossRef](#)]
6. Castro, J.M.; Macosko, C.W. Studies of mold filling and curing in the reaction injection molding process. *AIChE J.* **1982**, *28*, 250–260. [[CrossRef](#)]
7. Heinen, K. *Mikrostrukturelle Orientierungszustände Strömender Polymerlösungen und Fasersuspensionen*; Universität Dortmund: Dortmund, Germany, 2007.
8. Autodesk. *Autodesk Simulation Moldflow Insight, Fundamentals 2014, Student Guide—Theory and Concepts Manual*; Ascent: Charlottesville, VA, USA, 2013.
9. Autodesk. *Simulation Moldflow Insight, Fundamentals 2014, Student Guide—Practice Manual*; Ascent: Charlottesville, VA, USA, 2013.
10. Autodesk. *Autodesk Simulation Moldflow Insight, Advanced Flow 2014, Student Guide—Theory and Concepts Manual*; Ascent: Charlottesville, VA, USA, 2013.
11. Tamil, J.; Ore, S.H.; Gan, K.Y. Molding Flow Modeling and Experimental Study on Void Control for Flip Chip Package Panel Molding with Molded Underfill Technology. *J. Microelectron. Electron. Packag.* **2012**, *9*, 19–30. [[CrossRef](#)]
12. Ospald, F. Numerical Simulation of Injection Molding using OpenFOAM. *Proc. Appl. Math. Mech.* **2014**, *14*, 673–674. [[CrossRef](#)]
13. Deshpande, S.S.; Anumolu, L.; Trujillo, M.F. Evaluating the performance of the two-phase flow solver interFoam. *Comput. Sci. Disc.* **2012**, *5*, 14–16. [[CrossRef](#)]

14. Marić, T.; Höpken, J.; Mooney, K. *The OpenFOAM Technology Primer*; Sourceflux: Duisburg, Germany, 2014; ISBN 978-3-00-046757-8.
15. Damián, S.M. *An Extended Mixture Model for the Simultaneous Treatment of Short and Long Scale Interfaces*; Universidad Nacional del Litoral: Santa Fe, Argentina, 2013.
16. Ruiz, E.; Waffo, F.; Owens, J. Modeling of resing cure kinetics for molding cycle optimization. In Proceedings of the 8th International Conference on Flow Process in Composite Materials, Douai, France, 11–13 July 2006.
17. Bernath, A.; Kärger, L.; Henning, F. Accurate Cure Modeling for Isothermal Processing of Fast Curing Epoxy Resins. *Polymers* **2016**, *8*, 390. [[CrossRef](#)]
18. Kamal, M.R.; Sourour, S. Kinetics and thermal characterization of thermoset cure. *Polym. Eng. Sci.* **1973**, *13*, 59–64. [[CrossRef](#)]
19. Liang, G.; Chandrashekhara, K. Cure kinetics and rheology characterization of soy-based epoxy resin system. *J. Appl. Polym. Sci.* **2006**, *102*, 3168–3180. [[CrossRef](#)]
20. Khalil Abdullah, M.; Abdullah, M.Z.; Mujeebu, M.A.; Kamaruddin, S. A Study on the Effect of Epoxy Molding Compound (EMC) Rheology during Encapsulation of Stacked-CHIP Scale Packages (S-CSP). *J. Reinf. Plast. Compos.* **2009**, *28*, 2527–2538. [[CrossRef](#)]
21. Khor, C.Y.; Abdullah, M.Z.; Lau, C.-S.; Azid, I.A. Recent fluid–structure interaction modeling challenges in IC encapsulation—A review. *Microelectron. Reliab.* **2014**, 1511–1526. [[CrossRef](#)]
22. Folgar, F.; Tucker, C.L. Orientation Behavior of Fibers in Concentrated Suspensions. *J. Reinf. Plast. Compos.* **1984**, *3*, 98–119. [[CrossRef](#)]
23. Advani, S.G.; Tucker, C.L. The Use of Tensors to Describe and Predict Fiber Orientation in Short Fiber Composites. *J. Rheol.* **1987**, 751–784. [[CrossRef](#)]
24. Advani, S.G.; Tucker, C.L. Closure approximations for three-dimensional structure tensors. *J. Rheol.* **1990**, 367–386. [[CrossRef](#)]
25. Skrabala, O.; Bonten, C. Orientierungsverhalten plättchenförmiger Zusatzstoffe in Kunststoff suspensionen. *J. Plast. Technol.* **2016**, 157–183. [[CrossRef](#)]



© 2018 by the authors. Licensee MDPI, Basel, Switzerland. This article is an open access article distributed under the terms and conditions of the Creative Commons Attribution (CC BY) license (<http://creativecommons.org/licenses/by/4.0/>).